

Peak Effect in Superconductors: Absence of Phase Transition and Possibility of Jamming in Vortex Matter*

Mahesh Chandran[†]

(Dated: October 30, 2019)

The magnetic field B dependence of the critical current I_c for a disordered superconductor is studied numerically at zero temperature. The $I_c(B)$ increases rapidly near the upper critical field B_{c2} , similar to the peak effect (PE) phenomenon observed in many superconductors. The real space configuration across the PE changes continuously from a partially ordered domain (polycrystalline) state into an amorphous state. The topological defect density $n_d(B) \sim e^{\alpha B^k}$ with $k > 1$. There is no evidence of a phase transition in the vicinity of the PE, suggesting that an order-disorder transition is not essential for the occurrence of the PE phenomenon. An alternative view is presented wherein the defective vortex configuration undergoes jamming at the onset of the PE. Remarkable similarity between the PE in vortex matter and the yield stress anomaly (YSA) in some solids is also discussed.

PACS numbers: 74.25.Qt, 74.25.Sv

I. INTRODUCTION

The critical current density J_c for type-II superconductors decreases monotonically as a function of the magnetic field B or the temperature T over most part of the B - T phase diagram. But quite often, a peak in the $J_c(B)$ (or $J_c(T)$) is observed close to the upper critical field $B_{c2}(T)$ (or critical temperature $T_c(B)$). This phenomenon is known as the peak effect (PE) and was first studied in 1961. Extensive work since then have shown that PE exist in wide class of materials, which includes low- T_c (Nb and its alloys[1], V_3Si [2], $NbSe_2$ [3]), high- T_c ($YBa_2Cu_3O_7$ [4]), heavy fermion (UPt_3 [5], UPd_2Al_3 [6]), and other exotic (Sr_2RuO_4 [7]) superconductors, including the recently discovered compound MgB_2 [8]. Apart from single crystals, the phenomenon have been observed in polycrystalline and thin amorphous films[9]. The PE is found to be more pronounced in the weak pinning limit and progressively diminishes with increasing pinning strength[10, 11]. An important characteristic of the PE phenomenon is the strong memory and history dependence of the vortex configuration, and have been observed in static and dynamic experiments[12, 13, 14, 15, 16, 17].

The theoretical explanation for the PE have changed over the years. The earliest explanation was based on the softening of the vortex lattice with increasing B [18]. If the vortex lattice rigidity falls more rapidly than the elementary vortex pinning strength f_p as $B \rightarrow B_{c2}$, the softening would allow vortices to conform to the random pinning potential better compared to a stiff vortex lattice. This idea was further developed and quantified in the

collective pinning theory by Larkin and Ovchinnikov[19] (LO). In the LO theory, the vortex lattice is broken into coherently pinned regions of volume $V_c = R_c^2 L_c$, where R_c and L_c are the transverse and the longitudinal correlation lengths, respectively. The V_c is related to the tilt modulus C_{44} and the shear modulus C_{66} of the vortex lattice. Within the LO theory, the critical current density $J_c \propto f_p(n_p/V_c)^{1/2}$. LO suggested that in 3D, the spatial dispersion of C_{44} can lead to exponential decrease in V_c near B_{c2} . If the elementary pinning strength f_p does not fall as rapidly as V_c , the collapse of V_c would cause J_c to rise thus giving the PE phenomenon. For 2D vortex system, PE is not expected within the LO theory since the only relevant elastic modulus C_{66} is weakly dispersive.

Experimentally, the PE have been observed in thin amorphous films (samples with thickness $d < L_c$). This was interpreted within the collective pinning theory as due to dimensional crossover from 2D to 3D in the pinning characteristic[20]. Recently, the PE have been observed in ultra thin Bi films of $d = 10A^\circ$ [21]. This is difficult to explain by dimensional crossover since that would require L_c to become less than $10A^\circ < \xi$, where ξ is the coherence length of the superconductor. Moreover, neutron scattering experiment on Nb crystal shows that L_c actually increases with B , and the decrease in L_c in the PE region is not appreciable[22]. The LO theory also runs into difficulty in explaining the PE in $J_c(T)$ [23].

The observation of topologically ordered vortex lattice on a length scale $r \gg R_c$ in high- T_c superconductors[24, 25] differed from the predictions of the LO theory. In LO theory, the positional correlation $C(r)$ decays exponentially. Detailed calculations showed that in the presence of weak point impurities a quasi-long range ordered vortex lattice survives in 3D with $C(r)$ decaying as a power-law[26, 27]. Such a phase has been termed as the Bragg glass (BG). The BG undergoes a first-order melting transition into a vortex liquid (VL) phase on increasing T . Increasing B above a characteristic field, topological defects are generated which transform the BG phase into the vortex glass (VG) phase[28]. The plastic deforma-

*This work was carried out during the authors' stay in the Department of Physics, University of California, Davis, 95616.

[†]Present Address: Materials Research Laboratory, John F Welch Technology Centre, GE India Technology Centre, Phase 2, Hoodi Village, Whitefield Road, Bangalore, 560066;
email address: mahesh.chandran@ge.com

tion caused by the topological defects in the VG leads to strong pinning, and hence higher J_c compared to the BG phase. The PE was thus interpreted as a consequence of a phase transition between the BG and the VG, or an order-disorder transition[29, 30]. Furthermore, the origin of anomalous dynamics near the PE was attributed to the coexistence of BG and VG phases in the vicinity of the transition[31, 32].

The PE phenomenon as an order-disorder transition has limitations. Firstly, the BG phase is not expected in 2D[33], and hence order-disorder transition cannot account for the PE in amorphous films. Secondly, the BG phase have been shown theoretically to exist in the presence of weak point impurities. It is not clear if the BG would survive in polycrystalline samples in which the PE have been well documented. Recent Bitter decoration of NbSe_2 across the PE shows no distinct ordered and disordered phases[34]. Also, the width of the field range in which the ordered and the disordered phases coexist have been shown to scale with the sample size, which is an evidence against the phase transition interpretation of the PE[35].

Attempts have been made to understand the PE phenomenon using numerical simulation. Cha and Fertig[36] used an attractive term in the inter-vortex potential to tune the C_{66} in 2D. A small peak in the total depinning force was observed which was associated with the transition from the elastic to plastic depinning. But as emphasized in Ref.[37], the peak in total depinning force as a function of C_{66} does not imply a peak in $J_c(B)$. Later simulation in 3D showed an insignificantly small peak near the BG to VG transition[38], compared to the large peaks observed in experiments. The PE was also studied in a model of layered superconductors where the peak in J_c was induced through the decoupling transition[39]. The simulations so far have failed to capture some of the basic characteristics of the PE phenomenon, for *e.g.* proximity of the phenomenon to the $B_{c2}(T)$ line.

In this paper, the behaviour of the critical current $I_c(B)$ for a 2D disordered vortex matter is studied using numerical simulation. The effect of finite vortex core is included in the inter-vortex interaction, and is shown to be essential for the realistic description of the system close to B_{c2} . The $I_c(B)$, which decreases monotonically in the intermediate field range, shows a rapid increase near B_{c2} in close agreement with the PE phenomenon observed in real systems. The vortex configuration shows no order-disorder transition but a continuous transformation from a polycrystalline domain state below the PE to a liquid-like amorphous state in the PE region. An alternative scenario for the PE is discussed where the vortex state undergoes jamming due to increased disorder. An empirical relation between the $I_c(B)$ and the real space defect density $n_d(B)$ is also obtained from the simulation which captures the essential physics governing the behaviour of $I_c(B)$ for a disordered vortex matter.

The paper is organized as follows: in section II, the simulation details are presented, followed by results in

section III. The results are discussed in Section IV, and the conclusions are summarized in Section V.

II. SIMULATION METHOD

Consider a 2D cross-section of a bulk type-II superconductor perpendicular to the magnetic field $\mathbf{B} = B\hat{\mathbf{z}}$. The vortices in 2D can be treated as classical particles interacting via two-body potential, and governed by an overdamped equation of motion

$$\eta \frac{d\mathbf{r}_i}{dt} = - \sum_{j \neq i} \nabla U_C^v(\mathbf{r}_i - \mathbf{r}_j) - \sum_k \nabla U^p(\mathbf{r}_i - \mathbf{R}_k) + \mathbf{F}_{ext}, \quad (1)$$

where, η is the flux-flow viscosity. The first term on the left hand side represents the inter-vortex interaction, and the second term is the attractive interaction between the vortex and the quenched impurities. \mathbf{F}_{ext} is the Lorentz force on the vortex due to an applied current. Each of the three terms are further discussed in detail below.

The inter-vortex potential $U_C^v(r) = \frac{\phi_0^2}{8\pi^2\lambda^2} K_0(\tilde{r}/\lambda)$, where K_0 is the modified Bessel function, and $\tilde{r} = (r^2 + 2\xi^2)^{1/2}$. ϕ_0 is the flux quantum, and λ and ξ are the penetration depth and the coherence length of the superconductor, respectively. This form of the interaction was derived by Clem from the Ginzburg-Landau (GL) equation using variational method[40, 41]. Conventionally, the vortex dynamics have been studied using the potential $U_L^v(r) = \frac{\phi_0^2}{8\pi^2\lambda^2} K_0(r/\lambda)$ which is derived from the London's equation. For small r , the $K_0(r) \propto -\ln(r)$, leading to an unphysical singularity in $U_L^v(r)$ as $r \rightarrow 0$. The potential $U_L^v(r)$ is thus inadequate for describing correctly the vortex core region which limits its applicability to small B . On the other hand, Clem's potential $U_C^v(r)$ is well behaved as $r \rightarrow 0$ and gives realistic form of the magnetic flux density $\mathbf{B}(r)$ and the supercurrent density $\mathbf{J}(r)$ near the vortex core region. The correct description of the vortex core region is essential to extend the simulation to high magnetic fields where the cores of the neighboring vortices tend to overlap. An important consequence of using Clem's potential is that the vortices are not point particles but has a finite radius ξ . This is an improvement over the previous simulations which treated vortices as point particles interacting via London's potential $U_L^v(r)$. It is also worth mentioning that the other approach for simulating the vortex dynamics close to B_{c2} is through the time dependent GL theory (TDGL). Unfortunately, the computation cost for TDGL is prohibitive even for a small sample size which restricts its utility[42]. The main objective of the present work is to obtain the correct qualitative behavior of the critical current at high fields which would help in understanding the mechanism of the PE. As the results show, the model represented by Eq.(1) embodies the necessary physics for that purpose.

The second term in Eq.(1) is the attractive force between the vortex and the quenched impurities which

act as pinning centers. The force is derived from the parabolic potential, $U^p(r) = U_0 \left(\frac{r^2}{r_p^2} - 1 \right)$ for $r < r_p$, and 0 otherwise. The impurities are randomly placed at positions \mathbf{R}_k in the simulation box. The third term is the Lorentz force $\mathbf{F}_{ext} = \frac{1}{c} \mathbf{J} \times \phi_0 \hat{\mathbf{z}}$ where \mathbf{J} is the current density. A uniform current density along the y -direction is assumed such that all vortices experience the same force F_{ext}^x along the x -direction. For the simulation purpose, the length is defined in units of $\lambda(B=0) = \xi_0$. The current density J and the velocity of the vortex v_x are in the units of cf_0/ϕ_0 and f_0/η , respectively, where $f_0 = \frac{\phi_0^2}{8\pi^2 \lambda_0^3}$. From the relation $\mathbf{E} = \mathbf{v} \times \mathbf{B}$, the $v_x \propto E_y \propto V$ where V is the voltage generated in the direction of the current $I \propto J_y \equiv F_{ext}^x$. Hence, the $v_x(F_{ext})$ behavior represents the $V(I)$ characteristic (or equivalently, $E(J)$ curve) of the superconductor.

The dimensionless magnetic field is defined as $b = B/B_{c2}$, where the upper critical field $B_{c2} = \frac{\phi_0}{2\pi\xi_0^2}$ and $\xi_0 = \xi(B=0)$. The b is calculated from the lattice constant $\frac{a_0}{\lambda_0} = \left(\frac{4\pi}{\sqrt{3}} \right)^{\frac{1}{2}} \left(\frac{1}{\kappa^2 b} \right)^{\frac{1}{2}}$. The GL parameter $\kappa = \frac{\lambda}{\xi}$ is an input to the simulation. In the GL theory, the length scale λ and ξ increases with b and diverges as $b \rightarrow 1$. The renormalization of λ and ξ with increasing b is included in the simulation through the relation $\lambda(b) = f(b)\lambda_0$ and $\xi(b) = f(b)\xi_0$, where $f(b) = 1/\sqrt{1-b^2}$. This form of $f(b)$ is similar to the T -dependence of ξ in the GL theory[43] with T/T_c replaced by $(B/B_{c2})^2$, and have been used previously in Ref.[44]. The same form of $f(b)$ is chosen for λ and ξ in order to keep κ B -independent.

The simulation was carried out by numerically integrating the equation of motion using the fourth order predictor-corrector scheme. Parallel algorithms were implemented to reduce the runtime, details of which can be found in Ref.45. For the initial state, a perfect vortex lattice driven by a large current $I \gg I_c$ was used. The I is then reduced to 0 in small steps and the average voltage V was calculated in the steady state at each step to obtain the $V(I)$ curve. In the dimensionless units defined above, the $V = I$ in the asymptotic limit $I \rightarrow \infty$. The I_c is defined as the current at which the $V \lesssim 10^{-5}$ [46]. The procedure used for obtaining the $V(I)$ curve was motivated by experiments where a stable vortex configuration is observed if the system is brought to rest after driven with $I \gg I_c$ [47]. Also, the $I_c(b)$ from such a method shows the largest peak compared to that obtained from the field-cooling experiments.

The real space configuration of vortices was characterized by locating the topological defects in the system using Delaunay triangulation. For the triangular vortex lattice, a topological defect is the vortex with coordination number other than 6. The defect density n_d/λ_0^2 is defined as the number of defects per unit area of the simulation box. Most of the defects form dislocations which are bound pair of vortices with coordination 5 and 7 (disclinations). The fraction of free disclination is small over a wide range of fields, and hence $n_d \approx 2n_{disl}$ where n_{disl} is the dislocation density. Along with the $V(I)$ curve, the

behaviour of $n_d(I)$ was also determined for each value of b . The n_d discussed below represents the defect density at $I = 0$, unless specified otherwise.

The parameters used in the simulation are $\kappa = 10$ and $\lambda(B=0) = 1000\text{\AA}$. These values are typical of low- T_c superconductors, particularly NbSe₂. The periodic boundary conditions were imposed in both directions. The magnetic field b was varied by changing the size of the simulation box, keeping the number of vortices N_v fixed (for smaller system size, N_v is also allowed to vary between 800-1200). The results presented below are for $N_v = 4096$. The prefactor U_0 of the pinning potential $U^p(r)$ is distributed randomly between $\Delta \pm 0.01$ where $\Delta = \langle U_0 \rangle$. The simulation is restricted to point impurities with the range of the pinning potential $r_p = \xi_0$. The pin density $n_p = 2.315/\lambda_0^2$. The dilute limit of n_p is chosen keeping in mind that the PE is observed close to B_{c2} where the concentration of effective pinning centre is expected to be very small.

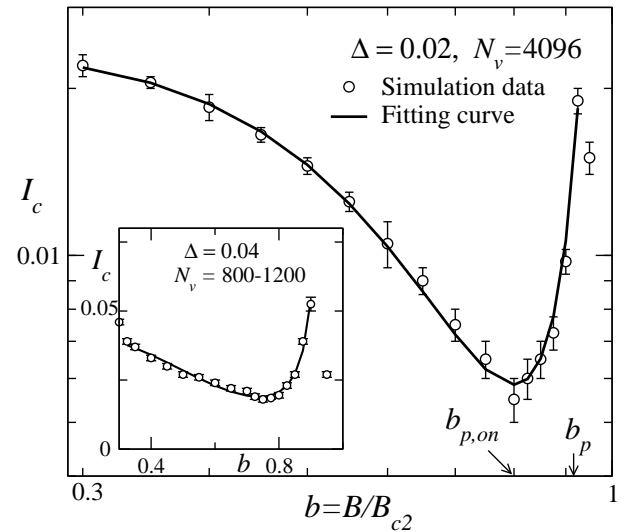


FIG. 1: The critical current $I_c(b)$ for $\Delta = 0.02$ and $N_v = 4096$. Inset: the $I_c(b)$ for $\Delta = 0.04$. For this plot, the N_v was also varied between 800 and 1200 along with the simulation box size. The thick line represents the fit to the simulation data (shown by open symbols).

III. RESULTS

A. Critical current $I_c(b)$

Figure 1 shows the $I_c(b)$ for $\Delta = 0.02$. For $b < b_{p,on} = 0.8$, the I_c decreases monotonically. At $b_{p,on}$, the $I_c(b)$ turns around and rises rapidly till $b = 0.925$. The rapid increases in I_c above $b_{p,on}$ signals the appearance of the PE. The inset shows the PE for $\Delta = 0.04$ for which a smaller system size was used. The $b_{p,on}$ decreases from a value of 0.9 for $\Delta = 0.01$ to 0.75 for $\Delta = 0.04$. The proximity of the PE to the upper critical field B_{c2} is in

good agreement with the experiments.

For $b > b_p = 0.925$, the I_c decreases. For $b \geq 0.95$, two vortices occasionally come together to form an effective vortex with charge $2\phi_0$. Overlapping of the two vortex cores is strongly influenced by the impurities. This was confirmed by simulating without the pinning centres where no overlapping of the vortices was found up to $b = 0.98$. The effective interaction between a $2\phi_0$ vortex and the ϕ_0 vortex is greater than the interaction between ϕ_0 vortices. This enhances the local rigidity of the vortex system, and is possibly the reason for the decrease in I_c . It is worth mentioning that a short range attractive interaction exist between the vortex cores[41] which is not included in the simulation. Such an interaction favors overlapping of the cores so as to gain the condensation energy, and becomes important as $B \rightarrow B_{c2}$. The important point is that the overlapping of vortex cores is observed for $b \geq 0.95$, and hence does not influence the increasing branch of the PE. It is possible that the $I_c(b)$ above b_p is influenced by the overlapping of vortices, a issue which can be addressed only by solving TDGL equations in the presence of impurities.

Attempts were made to fit the $I_c(b)$ data to a single function across the PE. A reasonably good fit was obtained using the expression

$$I_c(b) = I_{c0} \exp(-\beta b^k) \frac{1}{(1-b^2)^4}, \quad (2)$$

with $k \approx 2.6$ and $\beta \approx 9.75$ for $\Delta = 0.02$. For $\Delta = 0.04$, $k \approx 2.4$ and $\beta \approx 8.3$. The above function was motivated by the behaviour of the $n_d(b)$ which follows the same exponential form, whereas the dependence on $\frac{1}{(1-b^2)}$ reflects the behaviour of λ and ξ as $b \rightarrow 1$. The renormalization of the length scales λ and ξ leads to weak inter-vortex interaction, and explains why the PE in real system occurs close to the $B_{c2}(T)$ line. As shown below, the bare length scale λ_0 and ξ_0 leads to a stiff vortex lattice for $b > 0.6$, and consequently the PE is absent.

B. $V(I)$ characteristics across the Peak Effect

Figure 2 shows the $V(I)$ curves across the PE. The curves for high- b crosses the curves for low- b in the sub-ohmic region. The crossing can be understood from the dynamics close to I_c . For $I \gtrsim I_c$, the dynamics is heterogeneous with few vortices moving in channels in a background of defective vortex configuration[48, 49, 50]. The width of the channels $\sim a_0$ and display large transverse wandering relative to the direction of the Lorentz force. Since not all vortices are active, the voltage response is sub-ohmic. The number of active channels increases with I , and for $I = I_p$ all vortices move in channels which are ordered transverse to the flow direction. The time-averaged defect density shows an abrupt drop at I_p , and represents annealing of the plastic deformation (some dislocations with Burger vector parallel to the Lorentz force can exist for $I > I_p$). For $I > I_p$, the response is ohmic

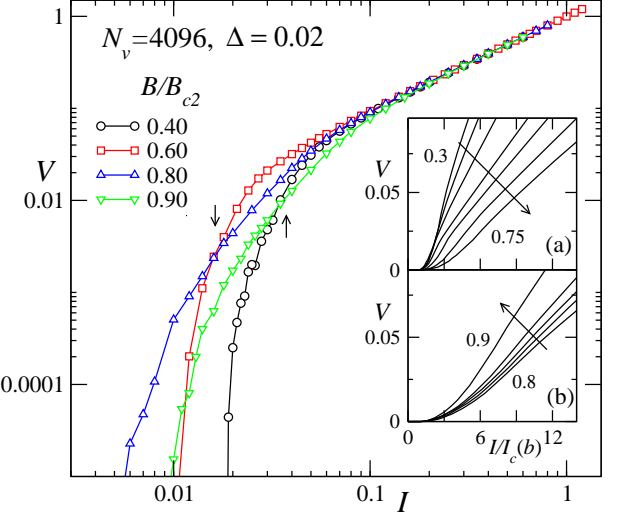


FIG. 2: The $V(I)$ curve across the PE. Arrows point to the crossing of $V(I)$ curves. Inset: the $V(I/I_c(b))$ curves for (a) $b < b_{p,on}$, and for (b) $b \geq b_{p,on}$. The arrows represent the direction of increasing b . The magnetic fields in (a) are 0.3, 0.4, 0.5, 0.6, 0.65, 0.7 and 0.75. In (b), the b increases from 0.8 to 0.9 in steps of 0.025.

and the resistance approaches the free flux-flow value. The sub-ohmic response window $\delta I_{dis} = I_p - I_c$ thus quantify the extent of plastic deformation of the vortex system. As shown in Ref.[51], $\delta I_{dis}(b)$ increases rapidly in the PE region implying that larger currents are required to anneal the defects. This is reflected in the slow growth of $V(I)$ curve for high fields, which consequently cross the curves for low fields, as shown in Fig. 2. Note that the crossing of curves occurs even below the PE (see curves for $b=0.6$ and 0.8), and is a consequence of the increase in plastic deformations rather than the PE phenomenon.

The inset in Fig. 2 shows the change in $V(I)$ characteristics as b is varied across the PE. For each curve, the I is scaled by the respective $I_c(b)$. Far below the PE, the curves are convex for $I \gtrsim I_c$. As b approaches $b_{p,on}$, the curvature changes to concave. The concave part of the $V(I)$ curve indicates a slow growth of the response due to increased plasticity of the system, as discussed above. Interestingly, for $I/I_c(b) > 1$, the $V(b)$ reflects the non-monotonic behaviour of $I_c(b)$. Thus, the PE is characterized by static as well as dynamic changes in the system, and agrees very well with the conclusion from experiments[52].

C. Real space configuration

One of the advantages of simulation is that changes in the real space configuration can be followed and characterized precisely. This allows verifying theories based on configurational changes. Fig. 3 shows the real space images at $I = 0$ in a region of the simulation box as b is changed across $b_{p,on}$. The defects are marked by

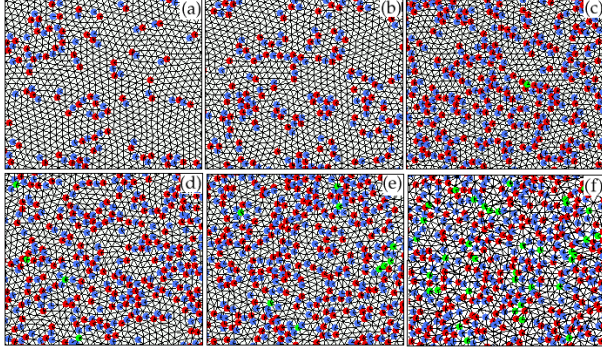


FIG. 3: The Delaunay triangulation of the real space configuration across $b_{p, on}$ for $b = 0.70$ (a), 0.75 (b), 0.80 (c), 0.85 (d), 0.875 (e), and 0.90 (f). The red and the blue dots represents vortices with 7 and 5 neighbors, respectively. The vortices with 4 and 8 neighbors are denoted by the green dot. The pinning strength $\Delta = 0.02$ and $N_v = 4096$. Only a small region of the simulation box is shown for clarity.

filled circles. A topologically ordered vortex lattice is not observed for any value of b consistent with the theory for 2D system[26]. But partial order can still be seen in large domains for $b \sim 0.4 - 0.6$. The dislocations are arranged in string-like structures and forms the grain boundary (domain walls). There are no free disclination below $b_{p, on}$. The configuration is reminiscent of a polycrystalline solid. With increasing b , the domain size decreases but the increase in the defect density occurs *within* the grain boundaries. Some of the domains can be seen for $b = 0.70$ and 0.75 . The average size of the domains decreases from $\approx 6a_0$ below the PE to $\approx 3a_0$ on the increasing branch of $I_c(b)$. At b_p , the configuration is amorphous (Fig. 3(d)) with defects forming a dense homogeneous network. It is not possible to isolate individual dislocations, and the configuration can be best described as that of a frozen liquid[54].

The continuous transformation of a less disordered state below $b_{p, on}$ into an amorphous state at b_p precludes an order-disorder (or BG to VG) transition underlying the PE. The PE is thought to be due to such a phase transition in the vortex system[29]. The real space images shown in Fig. 3 is strikingly similar to the recent Bitter decoration of NbSe₂ in the PE region, which lends support to the idea that a phase transition is not necessary for the PE to occur. The amorphous state at b_p is also consistent with the neutron scattering experiment[22] and the STM imaging of the vortices[55] in the PE region.

D. Defect density $n_d(b)$

Figure 4 shows the $n_d(b)$ at $I = 0$ for $\Delta = 0.02$ and $\Delta = 0.04$ (inset). As mentioned earlier, reducing I to zero from $I \gg I_c$ generates a configuration which is stable and does not show hysteresis[47]. The $n_d(I = 0)$ can

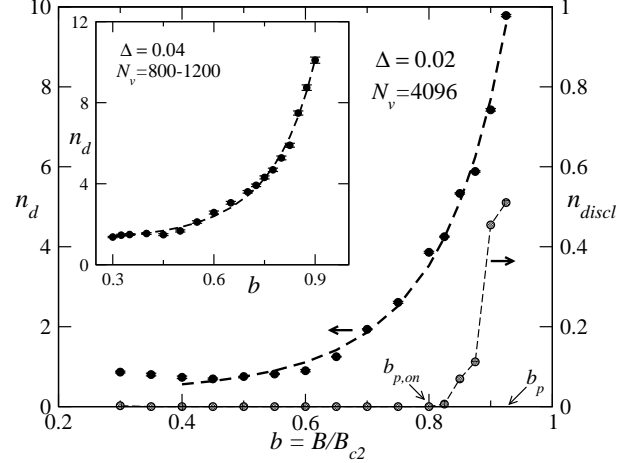


FIG. 4: The defect density n_d at $I = 0$ as a function of b . The thick dashed line is a fit to $n_d(b) = n_{d0} \exp(ab^k)$. The $n_{discl} = |n_{d,7} - n_{d,5}|$ can be considered as an approximation to the density of free disclinations, where $n_{d,7}$ and $n_{d,5}$ are the density of vortices with coordination number 7 and 5, respectively. Inset: the $n_d(b)$ plot for $\Delta = 0.04$. The thick dashed line is a fit to $n_d(b) = n_{d0} \exp(ab^k)$.

thus be considered as the equilibrium defect density and determines the behaviour of stable $I_c(b)$. The $n_d(b)$ for $b \gtrsim 0.4$ can be fit to

$$n_d(b) = n_{d0} \exp(ab^k), \quad (3)$$

with $\alpha \approx 3.9$ and $k \approx 2.6$ for $\Delta = 0.02$, and $\alpha \approx 3.0$ and the $k \approx 2.4$ for $\Delta = 0.04$. Interestingly, both $n_d(b)$ and $I_c(b)$ can be fit using the same value of k . For $\Delta = 0.02$, it is possible to write

$$I_c(b) = \frac{I_{c1}}{[n_d(b)]^{5/2}} \frac{1}{(1 - b^2)^4}, \quad (4)$$

where I_{c1} is the new coefficient. For $\Delta = 0.04$, the exponent $5/2$ changes to ≈ 2.7 . Figure 4 also shows the density of free disclinations which can be approximately defined as $n_{discl} = |n_{d,7} - n_{d,5}|$, where $n_{d,7}$ and $n_{d,5}$ are the density of vortices with coordination number 7 and 5, respectively. The n_{discl} is 0 for $b < 0.8$, and rises rapidly in the PE region suggesting a liquid-like configuration.

From the above analysis of the $n_d(b)$ and the $I_c(b)$ data, it is possible to conclude that $I_c(b) \propto [n_d(b)]^{-r}$, where the effect of the pinning potential is implicit through the defect density $n_d(b)$ and the exponent r . This empirical relation between $n_d(b)$ and $I_c(b)$ captures the essential physics governing the behaviour of the critical current in a disordered vortex system with point impurities. Physically, the increase in n_d with b enables plastic shearing to be initiated at lower currents, which explains the monotonic decrease in I_c below the PE. But this also leads to a paradoxical situation: since the $n_d(b)$ continues to rise rapidly even in the PE region, the enhanced plasticity of the system should cause the I_c to decrease continuously till B_{c2} , contrary to the observation of PE above

$b_{p, on}$. The problem is compounded further since the real space images do not suggest any noticeable configurational change across $b_{p, on}$ which can be associated with sudden increase in pinning due to quenched impurities.

The above paradox can be resolved by conjecturing that the vortex system undergoes jamming at the onset of the PE due to increase in n_d . The jamming envisaged here is similar to the jamming in granular materials where the system develops a finite yield stress at a threshold packing fraction[56]. The jamming in the vortex system could occur due to disordered packing of vortices which imposes kinematic constraint for the motion of vortices. It is observed that the defect fraction f_d , defined as the ratio of the number of defects to the total number of vortices, becomes 0.30 at $b_{p, on}$, which could possibly be the threshold value for the jamming to occur in the vortex system. As mentioned earlier, the dynamics close to the I_c is governed by few active channels. The effect of disordered packing of vortices is to increase the effective energy barrier ΔE_T for the transverse mobility of the channel, thus requiring larger current to initiate channel dynamics. Future work should be able to obtain the B -dependence of ΔE_T , which could provide evidence for jamming in the PE region.

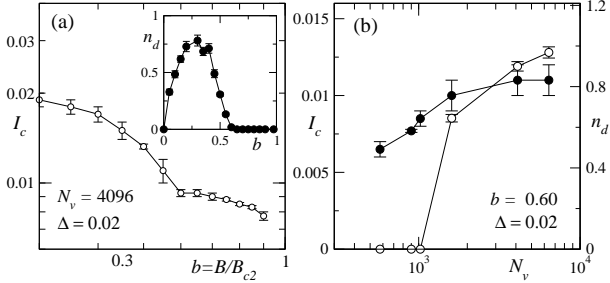


FIG. 5: (a) The $I_c(b)$ and $n_d(b)$ (inset) without the field dependence of the length scales λ and ξ . The $\Delta = 0.02$ and $N_v = 4096$. (b) Behavior of I_c and n_d as a function of N_v for $b = 0.6$ and $\Delta = 0.02$

E. Field independent λ and ξ

The $I_c(b)$ and the $n_d(b)$ obtained using $\lambda(b) = \lambda_0$ and $\xi(b) = \xi_0$ are shown in Fig. 5(a). The λ_0 and ξ_0 are the values at $B = 0$. For $b < 0.6$, the $I_c(b)$ does not show any appreciable deviation from that of Fig. 1. At $b \approx 0.6$, the defect density n_d becomes zero, and the system remains topologically ordered till B_{c2} . As a consequence, the PE is absent at high fields and is consistent with the idea that the PE cannot occur in rigid vortex lattice.

F. Finite size effect

The finite size effect on n_d and I_c was determined by increasing N_v for $b = 0.6$. The total number of defects

shows a minimum around $b = 0.60$, or equivalently, the average size of the ordered region (domain) is maximum for this field. Hence, any relevant length scale determining the system behaviour would be largest for $b = 0.6$. Figure 5(b) shows I_c and n_d as a function of the system size ($\propto N_v$). The maximum N_v which could be simulated was 6400. For $N_v \gtrsim 4000$, the I_c tends to become independent of the system size, though n_d appears to be increasing. The system size used in the simulation is thus sufficient to obtain macroscopic behaviour of the $I_c(b)$. Overall, the finite size effect demonstrates the necessity of going to larger system size for doing realistic simulation of the vortex dynamics.

IV. DISCUSSIONS

The results presented above provides evidence for the absence of phase transition at the PE in superconductors. This rules out any generic explanation based on order-disorder transition (or Bragg glass to vortex glass transition), and resolves the difficulty in interpreting the PE in thin amorphous films where an ordered (or Bragg glass) vortex phase cannot exist. The simulation results cannot be explained by invoking the softening of the vortex lattice as the mechanism for the PE. Along with increasing defect density in the vortex system, the inter-vortex interaction must become sufficiently weak for the PE to occur. As conjectured earlier, this could lead to jamming in the vortex system.

It is also possible to explain the anomalous dynamics in the PE region within the jamming scenario. Henderson *et al.* showed that the vortex system responds to a bi-directional current of amplitude $I < I_c$, but shows no response for dc or uni-directional current of the same amplitude[14]. The voltage response with bi-directional current grows with the number of pulses before saturating, suggesting a strong athermal component in the relaxation. Similar athermal behaviour is observed in the granular systems which undergoes relaxation on “tapping”. Experiments find logarithmic relaxation as a function of the number of taps for the compaction of the granular heap[57]. If the vortex system is indeed jammed in the PE region, a similar logarithmic relaxation can be expected with the time replaced by the number of “taps” applied to the system. The “tapping” of the vortex system can be done by applying a bi-directional current pulse just below the I_c , or a small ac-field in magnetization measurement in the PE region.

Recently, in an interesting experiment, Ravikumar *et al.* measured the magnetic relaxation in V_3Si in the PE region[58]. The authors recorded the data at regular intervals of 200 and 600 seconds. They discovered that if the magnetic moment M is plotted as a function of serial number of measurement n rather than the real time, the two data set collapses on the same curve, even though the total time of relaxation is different for the two data sets. If the serial number n is assumed to be the number

of “taps” applied to the system[59], the athermal relaxation observed in the experiment is an evidence in favor of jamming of the vortex matter in the PE region.

The disordered vortex matter under Lorentz force shows close analogy to solids under stress. It then becomes relevant to seek an analogous phenomenon to the PE in vortex matter. In the field of metallurgy, it is known that for some solids the yield stress increases with T before sharply decreasing, and is referred as the yield stress anomaly (YSA)[60]. In a naive picture, the yield stress is expected to decrease monotonically with T , since increasingly more mobile dislocations are activated at higher temperatures. The YSA have been observed in disordered alloys, steel, and in some case even in pure metals. The equivalence of yield stress for solids and the critical current density for the vortex matter implies a strong underlying commonality between YSA and the PE. In some intermetallic alloys (Cu_3Au), the YSA occurs just below the order-disorder transition and have been linked to phase transition, in resonance with one of the interpretation for PE. Also, anomalous dynamics is observed in the region of YSA, including jerky motion of the dislocations, similar to the dynamics of vortices in the PE region. There is no single interpretation for YSA which can be applied to all systems, but it is agreed that the phenomenon is closely related to the kinematic constraints on dislocation dynamics.

The similarity between the YSA and the PE suggests that the anomalous dynamics in the PE region can be understood by studying dislocation dynamics in the vortex matter. The jamming have been recently studied in dislocation network formed in a plastically deformed material[61], and can be used as a model system for studying the vortex dynamics in the PE region. The

dislocation network also shows complex spatio-temporal dynamics[62] with strong history dependence and memory effect.

V. CONCLUSIONS

The paper describes the results from detailed simulation of the magnetic field dependence of I_c for a superconductor at $T = 0$. The $I_c(B)$ shows a large peak near the upper critical field B_{c2} , in agreement with the experimental observation of the peak effect phenomenon. There is no evidence of a phase transition in the peak effect region. Instead, a continuous transformation of a less disordered state into an amorphous state is observed, implying that an ordered state is not necessary for the PE to occur. A jamming scenario is presented which could explain the PE, and can account for the anomalous dynamics in the peak effect region of the $I_c(B)$ plot. Attention is drawn to the close analogy between the PE in vortex matter and the yield stress anomaly (YSA) in solids.

Acknowledgments

M.C. acknowledges useful discussions with A. K. Grover, E. Zeldov, S. Bhattacharya, and Ravi Kumar during various stages of the work, and thanks G. T. Zimanyi and R. T. Scalettar for critical comments during the early part of the work. The simulation was performed at the Albuquerque High Performance Computing Center, University of New Mexico, during the authors’ stay at the University of California, Davis.

[1] T. G. Berlincourt, R. R. Hake, and D. H. Leslie, Phys. Rev. Lett. **6**, 671 (1961). See also W. DeSorbo, Rev. Mod. Phys. **36**, 90 (1964).

[2] M. Isino, T. Kobayashi, N. Toyota, T. Fukase, and Y. Muto, Phys. Rev. B **38**, 4457 (1988).

[3] M. J. Higgins and S. Bhattacharya, Physica C **257**, 232 (1996) and references there in.

[4] G. D’Anna, M. V. Indenbom, M.-O. Andr, W. Benoit, and E. Walker, Europhys. Lett. **25**, 225 (1994); D. Pal, D. Dasgupta, B. K. Sarma, S. Bhattacharya, S. Ramakrishnan, and A. K. Grover, Phys. Rev. B **62**, 6699 (2000).

[5] K. Tenya, M. Ikeda, T. Tayama, H. Mitamura, H. Amitasu, T. Sakakibara, K. Maezawa, N. Kimura, R. Settai, and Y. Onuki, J. Phys. Soc. Jap. **64**, 1063 (1995).

[6] A. Ishiguro, A. Sawada, Y. Inada, J. Kimura, M. Suzuki, N. Sato, and T. Komatsubara, J. Phys. Soc. Jap. **64**, 378 (1995).

[7] T. Tamegai, K. Behnia, N. Okuda, S. Ooi, T. Shibauchi, Z. Mao, and Y. Maeno, Physica B **284**, 543 (2000).

[8] M. Pissas, S. Lee, A. Yamamoto, and S. Tajima, Phys. Rev. Lett. **89**, 097002 (2002).

[9] R. Wördenweber, P. H. Kes, and C. C. Tsuei, Phys. Rev. B, **33**, 3172 (1986) and references there in.

[10] S. S. Banerjee, S. Ramakrishnan, A. K. Grover, G. Ravikumar, P. K. Mishra, V. C. Sahni, C. V. Tomy, G. Balakrishnan, D. Mck. Paul, P. L. Gammel, D. J. Bishop, E. Bucher, M. J. Higgins, and S. Bhattacharya, Phys. Rev. B **62**, 11838 (2000).

[11] E. Y. Andrei, Z. L. Xiao, W. Henderson, Y. Paltiel, E. Zeldov, M. Higgins, S. Bhattacharya, P. Shuk, and M. Greenblatt, Condensed Matter Theories **16**, 241 (2001).

[12] J. A. Good and E. J. Kramer, Phil. Mag. **24**, 339 (1971).

[13] Z. L. Xiao, E. Y. Andrei, and M. J. Higgins, Phys. Rev. Lett. **83**, 1664 (1999).

[14] W. Henderson, E. Y. Andrei, and M. J. Higgins, Phys. Rev. Lett. **81**, 2352 (1998).

[15] S. O. Valenzuela and V. Bekeris, Phys. Rev. Lett. **84**, 4200 (2000); *ibid.* **86**, 504 (2001).

[16] S. B. Roy, P. Chaddah, and P. Chaudhary, Phys. Rev. B **62**, 9191 (2000).

[17] S. S. Banerjee, N. G. Patil, S. Ramakrishnan, A. K. Grover, S. Bhattacharya, G. Ravikumar, P. K. Mishra, T. V. Chandrasekhar Rao, V. C. Sahni, and M. J. Higgins, Appl. Phys. Lett. **74**, 126 (1999).

[18] A. B. Pippard, *Phil Mag.* **19**, 217 (1969).

[19] A. I. Larkin, and Yu. N. Ovchinnikov, *J. Low. Temp. Phys.* **34**, 409 (1979).

[20] P. H. Kes and C. C. Tsuei, *Phys. Rev. B* **28**, 5126 (1983); P. Koorevaar, J. Aarts, P. Berghuis, and P. H. Kes, *Phys. Rev. B* **42**, 1004 (1990).

[21] G. Sambandamurthy, K. Das Gupta, and N. Chandrasekhar, *Phys. Rev. B* **63**, 214519 (2001).

[22] P. L. Gammel, U. Yaron, A. P. Ramirez, D. J. Bishop, A. M. Chang, R. Ruel, L. N. Pfeiffer, E. Bucher, G. D'Anna, D. A. Huse, K. Mortensen, M. R. Eskildsen, and P. H. Kes, *Phys. Rev. Lett.* **80**, 833 (1998).

[23] X. Ling, C. Tang, S. Bhattacharya, and P. M. Chaikin, *Europhys. Lett.* **35**, 597 (1996).

[24] D. G. Grier, C. A. Murray, C. A. Bolle, P. L. Gammel, D. J. Bishop, D. B. Mitzi and A. Kapitulnik, *Phys. Rev. Lett.* **66**, 2270 (1991).

[25] E. M. Forgan, D. McK. Fault, H. A. Mook, P. A. Timmins, H. Keller, S. Sutton, and J. S. Abell, *Nature* **343**, 735 (1990).

[26] T. Giamarchi and P. Le Doussal, *Phys. Rev. Lett.* **72**, 1530 (1994); *Phys. Rev. B* **52**, 1242 (1995).

[27] T. Nattermann and S. Scheidl, *Adv. Phys.* **49**, 607 (2000).

[28] T. Giamarchi and P. Le Doussal, *Phys. Rev. B* **55**, 6577 (1995).

[29] Y. Paltiel, E. Zeldov, Y. Myasoedov, M. L. Rappaport, G. Jung, S. Bhattacharya, M. J. Higgins, Z. L. Xiao, E. Y. Andrei, P. L. Gammel, and D. J. Bishop, *Phys. Rev. Lett.* **85**, 3712 (2000).

[30] G. Ravikumar, V. C. Sahni, A. K. Grover, S. Ramakrishnan, P. L. Gammel, D. J. Bishop, E. Bucher, M. J. Higgins, and S. Bhattacharya, *Phys. Rev. B* **63**, 024505 (2001).

[31] M. Marchevsky, M. J. Higgins, and S. Bhattacharya, *Nature* **409**, 591 (2001).

[32] Y. Paltiel, E. Zeldov, Y. N. Myasoedov, H. Shtrikman, S. Bhattacharya, M. J. Higgins, Z. L. Xiao, E. Y. Andrei, P. L. Gammel, and D. J. Bishop, *Nature* **403**, 398 (2000).

[33] C. Zeng, P. L. Leath, and D. S. Fisher, *Phys. Rev. Lett.* **82**, 1935 (1999).

[34] Y. Fasano, M. Menghini, F. de la Cruz, Y. Paltiel, Y. Myasoedov, E. Zeldov, M. J. Higgins, and S. Bhattacharya, *Phys. Rev. B* **66**, 020512(R) (2002).

[35] R. Schleser, P. J. E. M. van der Linden, P. Wyder, and A. Gerber, *Phys. Rev. B* **67**, 134516 (2003).

[36] Min-Chul Cha and H. A. Fertig, *Phys. Rev. Lett.* **80**, 3851 (1998).

[37] C. Reichhardt, K. Moon, R. Scalettar, and G. T. Zimányi, *Phys. Rev. Lett.* **83**, 2282 (1999).

[38] A. van Otterlo, R. T. Scalettar, and G. T. Zimányi, R. Olsson, A. Petrean, W. Kwok, and V. Vinokur, *Phys. Rev. Lett.* **84**, 2493 (2000).

[39] C.J. Olson, C. Reichhardt, R.T. Scalettar, G.T. Zimányi, and N. Grønbech-Jensen, *Physica C*, **384**, 143 (2003).

[40] J. R. Clem, *J. Low. Temp. Phys.* **18**, 427 (1975); Z. Hao and J. R. Clem, M. W. McElfresh, L. Civale, A. P. Malozemoff, and F. Holtzberg, *Phys. Rev. B* **43**, 2844 (1991).

[41] E. H. Brandt, *Rep. Prog. Phys.* **58**, 1465 (1995).

[42] G. W. Crabtree, D. O. Gunter, H. G. Kaper, A. E. Koshelev, G. K. Leaf, and V. M. Vinokur, *Phys. Rev. B* **61**, 1446 (2000).

[43] M. Tinkham, *Introduction to Superconductivity*, McGraw Hill, New York (1975).

[44] S. Ryu and D. Stroud, *Phys. Rev. B* **54**, 1320 (1996).

[45] Mahesh Chandran, cond-mat/0103263.

[46] The I_c can also be defined as the current at which the dynamic resistance $\frac{dV}{dI}$ first becomes 0 as I is reduced. The I_c from this definition does not differ more than 2σ from the criterion used, where σ is the step by which the current is changed in obtaining the $V(I)$ curve around I_c .

[47] W. Henderson, E. Y. Andrei, M. J. Higgins and S. Bhattacharya, *Phys. Rev. Lett.* **77**, 2077 (1996).

[48] H. J. Jensen, A. Brass, and A. J. Berlinsky, *Phys. Rev. Lett.* **60**, 1676 (1988); H. J. Jensen, A. Brass, A. Shi, and A. J. Berlinsky, *Phys. Rev. B* **41**, 6394 (1990).

[49] C. J. Olson, C. Reichhardt, and F. Nori, *Phys. Rev. Lett.* **81**, 3757 (1998).

[50] N. Grønbech-Jensen, A. R. Bishop, and D. Domínguez, *Phys. Rev. Lett.* **76**, 2985 (1996).

[51] Mahesh Chandran, R. T. Scalettar, and G. T. Zimányi, *Phys. Rev. B* **67**, 052507 (2003).

[52] S. Bhattacharya and M. J. Higgins, *Phys. Rev. Lett.* **70**, 2617 (1993).

[53] Mahesh Chandran, R. T. Scalettar, and G. T. Zimányi, *Phys. Rev. B* **69**, 024526 (2004).

[54] Similar amorphous regime exists for low fields ($b \rightarrow 0$), as discussed in Ref.[53].

[55] A. M. Troyanovski, M. van Hecke, N. Saha, J. Aarts, and P. H. Kes, *Phys. Rev. Lett.* **89**, 147006 (2002).

[56] C. S. O'Hern, L. E. Silbert, A. J. Liu, and S. R. Nagel, cond-mat/0304421.

[57] J. B. Knight, C. G. Fandrich, C. N. Lau, H. M. Jaegar, and S. R. Nagel, *Phys. Rev. E* **51**, 3957 (1995).

[58] G. Ravikumar, M. R. Singh, and H. Küpfer, cond-mat/0309494.

[59] In Ref.[58], the magnetization M was measured in a SQUID magnetometer where the sample undergoes excursion in a small inhomogeneous field. This creates a small driving current during the excursion of the sample which is restricted near the surface of the sample. The Lorentz force due to this additional current can be thought as providing the “tapping” force for the vortex system.

[60] D. Caillard, *Mat. Sci. and Engg.* **A319**, 74 (2001), and references there in.

[61] M.-Carmen Miguel, A. Vespignani, M. Zaiser, and S. Zapperi, *Phys. Rev. Lett.* **89**, 165001 (2002); M.-Carmen Miguel, J. S. Andrade Jr., S. Zapperi, cond-mat/0304555 (unpublished).

[62] G. D' Anna, and F. Nori, *Phys. Rev. Lett.* **85**, 4096 (2000).